Journal of Power Sources 193 (2009) 713–722

Contents lists available at ScienceDirect

Journal of Power Sources

journal homepage: www.elsevier.com/locate/jpowsour

# Method using gas chromatography to determine the molar flow balance for proton exchange membrane fuel cells exposed to impurities

G. Bender*, M. Angelo, K. Bethune, S. Dorn, T. Thampan[1], R. Rocheleau

*University of Hawaii, Hawaii Natural Energy Institute, 1680 East West Road POST 109, Honolulu, HI 96822, USA*

ARTICLE INFO

*Article history:*
Received 5 February 2009
Received in revised form 17 April 2009
Accepted 17 April 2009
Available online 23 April 2009

*Keywords:*
PEMFC
Fuel cell
Impurity
Gas analysis
Molar flow balance
Gas chromatography

ABSTRACT

An understanding of the potentially serious performance degradation effects that trace level contaminants can cause in proton exchange membrane fuel cells (PEMFCs) is crucial for the successful deployment of PEMFC for commercial applications. An experimental and analytic methodology is described that employs gas chromatography (GC) to accurately determine the concentration of impurity species in the fuel and oxidant streams of a PEMFC. In this paper we further show that the accurate determination of the contaminant concentrations at the anode and cathode inlets and outlets provides a means to quantify reactions of contaminants within the cell and to identify diffusive mass transport across the membrane. High data accuracy down to sub-ppm contaminant levels is required and was achieved by addressing several challenges pertaining to experimental setup and data analysis which are both discussed in detail. The application of the methodology is demonstrated using carbon monoxide and toluene which were injected into the cell at concentrations between 1 and 10 ppm and 20 and 60 ppm, respectively. Both impurities were observed to react in the fuel cell: carbon monoxide to carbon dioxide, and toluene to methylcyclohexane. For both contaminants closure of the molar flow balances to within 3% was achieved even at the low contaminant concentrations. This allowed the extent of both reactions at the applied operating conditions to be quantified. The presented methodology is shown to be a valuable tool for investigating the effects and reactions of trace contaminants in fuel cells and for providing critical insights into the mechanisms responsible for the associated performance degradation.



## 1. Introduction

Proton exchange membrane fuel cells (PEMFCs) are energy conversion devices that offer high power densities at low operating temperatures. These advantages make PEMFCs the most promising technology for many transient applications such as fuel cell powered automobiles, back-up power generating units, and portable devices. While the low operating temperature of PEMFCs allows quick start-up and rapid response to energy demand, it can also cause stronger adsorption of contaminants on the anode and cathode catalyst surfaces. This may result in serious degradation of cell performance even in the presence of trace amounts of fuel or air contaminants.

Carbon monoxide (CO), which is a common hydrogen ($H_2$) fuel contaminant has been extensively investigated using ex situ [1–12] and in situ [13–18] methods with CO partial pressures ranging from 10 to 100 ppm. The existing impurity studies were often accompanied by modeling efforts to describe and explain the poisoning phenomena for CO on the platinum surface [1,19–22]. Recently developed guidelines for hydrogen fuel quality, however, recommend impurity concentrations far below the values typically used in these studies [23]. Other anode impurities such as carbon dioxide ($CO_2$), hydrogen sulfide ($H_2S$), and ammonia ($NH_3$) have also been investigated [1,18,24–30]. On the cathode, trace levels of contaminants in the feed stream such as sulfur oxides ($SO_X$) and nitrous oxides ($NO_X$) have been shown to impact the fuel cell performance [5,31–34]. These impurities originate from air pollution or other challenging environments such as battlefield scenarios [5,34].

Most of the in situ impurity studies reported in the literature were performed by injecting impurity containing gas into the anode or cathode feed stream while monitoring the performance response of the cell [13–17,19]. In other cases, diagnostic methods includ-

*Abbreviations:* BOT, beginning of test; EIS, electrochemical impedance spectroscopy; EOT, end of test; FC, fuel cell; FID, flame ionization detector; GC, gas chromatography; GC–MS, gas chromatograph/mass spectrometry; GDL, gas diffusion layer; HOR, hydrogen oxidation reaction; MEA, membrane electrode assembly; OEM, original equipment manufacturer; ORR, oxygen reduction reaction; PDID, pulsed discharge ionization detector; PEMFC, proton exchange membrane fuel cell; PFPD, pulsed flame photometric detector; PSA, pressure swing adsorption; SPME, solid phase microextraction adsorption; TCD, thermal conductivity detector; WG12, ISO TC 197 Working Group 12.

* Corresponding author. Tel.: +1 808 956 0877; fax: +1 808 956 2344.
*E-mail address:* gbender@hawaii.edu (G. Bender).
[1] Current address: American Air Liquide, Newark, DE 19702, USA.

0378-7753/$ – see front matter © 2009 Elsevier B.V. All rights reserved.
doi:10.1016/j.jpowsour.2009.04.028

**Nomenclature**

| | |
|---|---|
| $I$ | cell current (A) |
| $P_{Cell}$ | cell pressure ($kPa_{abs}$) |
| $\Delta H$ | change in enthalpy of solution ($J\,mol^{-1}$) |
| $Q_{CBal}$ | closure of carbon balance (%) |
| $c_i$ | concentration of species $i$ dissolved in liquid ($mol\,dm^{-3}$) |
| $a_{CO_2}$ | conversion factor for $CO_2$ (ppm to $mol\,s^{-1}$) |
| $a_i$ | conversion factor for impurity (ppm to $mol\,s^{-1}$) |
| $F$ | Faraday's constant ($C\,mol^{-1}$) |
| $\lambda$ | flow stoichiometry |
| $\alpha$ | fraction of fuel or oxidant in reaction gas stream |
| $k^0_{H,i}$ | Henry's constant at reference conditions ($mol\,dm^{-3}\,atm^{-1}$) |
| $k_{H,i}$ | Henry's constant for species $i$ ($mol\,dm^{-3}\,atm^{-1}$) |
| $R$ | ideal gas constant ($J\,mol^{-1}\,K^{-1}$) |
| $\bar{\dot{n}}_{i,in}$ | molar flow rate average of carbon containing compounds entering the cell ($mol\,s^{-1}$) |
| $\bar{\dot{n}}_{i,out}$ | molar flow rate average of carbon containing compounds exiting the cell ($mol\,s^{-1}$) |
| $\dot{n}_{g,M}$ | molar flow rate of clean gas in main gas stream ($mol\,s^{-1}$) |
| $\dot{n}_{CO_2}$ | molar flow rate of $CO_2$ ($mol\,s^{-1}$) |
| $\dot{n}_i$ | molar flow rate of impurity gas ($mol\,s^{-1}$) |
| $\dot{n}_{g,I}$ | molar flow rate of injected impurity/carrier gas mixture ($mol\,s^{-1}$) |
| $\dot{n}_{r,In}$ | molar flow rate of reactant gas into FC ($mol\,s^{-1}$) |
| $\dot{n}_{r,Out}$ | molar flow rate of reactant gas out of FC ($mol\,s^{-1}$) |
| $\dot{n}_{w,act,In}$ | molar flow rate of water actually entering the FC ($mol\,s^{-1}$) |
| $\dot{n}_{w,Hyp}$ | molar flow rate of water entering fuel cell assuming water trap of equivalent effectiveness placed in feed stream to FC ($mol\,s^{-1}$) |
| $y_{CO_2,ppm}$ | mole fraction of $CO_2$ (ppm) |
| $y_{i,ppm}$ | mole fraction of impurity (ppm) |
| $y_{w,In/Out}$ | mole fraction of water in inlet or outlet streams |
| $n$ | number of electrons transferred during electrochemical reaction |
| $p_i$ | partial pressure of species $i$ over liquid (atm) |
| $\phi$ | relative humidity |
| $P^{Sat}_w(T_{Cell})$ | saturation pressure of water as a function of cell temperature ($kPa_{abs}$) |
| $P^{Sat}_w(T_H)$ | saturation pressure of water as a function of humidifier temperature ($kPa_{abs}$) |
| $T_{Sat}$ | saturation temperature of gas exiting FC (°C) |
| $T_C$ | temperature of fuel cell (°C) |
| $T_H$ | temperature of humidifier (°C) |
| $T$ | temperature of system (°C) |
| $T^0$ | temperature reference (25 °C) |

ing cyclic voltammetry or electrochemical impedance spectroscopy (EIS were employed to identify and quantify the amounts of residual impurity species adsorbed onto the catalyst surface [16,27,30]) and to identify the mechanism for the overpotential increase [35]. While these studies have produced important results pertaining to the effect of contaminants on fuel cell performance, little has been done to characterize gas composition during fuel cell operation with impurity exposure [31,36]. Furthermore, the studies that have considered gas stream composition typically analyzed only one exhaust gas stream. Conclusions derived with this methodology relied on the assumption that the compositions of the unmonitored gas streams were known and that interaction between anode and cathode gas streams were negligible although some reports have suggested otherwise [37,38].

In this paper, we describe an experimental and analytic methodology that employs gas chromatography (GC) to accurately determine the concentration of impurity species in the fuel and oxidant streams of a PEMFC. Careful analysis of the carryover of water from the cell to the GC was essential to be able to quantify gas concentrations to sub-ppm levels. We show that careful measurement and analysis of contaminants at the inlet and outlet streams of the anode and cathode allows closure of the molar flow balances under steady state conditions and provides a means to identify and quantify reactions within the cell and to estimate diffusive mass transport across the membrane. Results of experiments with CO concentrations between 1 and 10 ppm and toluene concentrations of 20 and 60 ppm in the $H_2$ inlet stream are presented.

## 2. Experimental

Testing was performed at the Hawaii fuel cell test facility (HFCTF), a state of the art laboratory for fuel cell testing and research on single cells and short stacks. The facility has on-site $H_2$ production, on-site air supply and purification, and a wide range of diagnostic equipment. Experiments for this work were conducted using UTC XTC 800 test stands modified for use with pressurized cells and Green Light Power FCATS™ G50 series test stations.

Fig. 1 shows a schematic of the gas flow, pressure, and temperature controls of the experimental apparatus used to inject and sample contaminants in the fuel and oxidant streams of the fuel cell. While the impurity is only introduced into the anode side for this work, identical gas sampling ports, pressure and temperature monitoring points, and back pressure control were also present on the cathode side of the fuel cell. Notable in Fig. 1 are four distinct temperature control zones used to ensure accurate control of cell humidification, gas inlet temperature, cell operating temperature, and gas temperature at the exit of the fuel cell. The humidification and temperature control systems had to be optimized and carefully controlled to maintain a small signal to noise ratio of the cell performance data during the 100-plus hour experiments.

As shown schematically in Fig. 1, contaminant gases were introduced into the fuel by injecting a dry $H_2$ stream containing the contaminant of interest into the main humidified fuel flow. Gas flows were controlled using digital mass flow controllers from Brooks or Bronkhorst calibrated with a BIOS International ML-800 dry gas piston flow calibrator, with an absolute accuracy of ±0.2% of the gas flow. The flow rate of $H_2$ in the main gas stream and that of the contaminated $H_2$ were metered to maintain both the desired contaminant level and the appropriate fuel stoichiometry at the anode. The relative humidity of the combined feed stream was controlled by increasing the humidifier temperature to compensate for the non-humidified contaminated $H_2$ gas injected just before the cell inlet.

The fuel and oxidant gases were humidified in control zone 1 (Fig. 1) to the desired relative humidity using the temperature controlled humidification units provided with the test stations. Saturation at the exit of the humidifiers was verified over the applied range of operating conditions using an Optidew vision chilled mirror hygrometer from Michell instruments. Under saturation conditions at the humidifier, the partial pressure of water $P^{Sat}_w(T_H)$ and thus the humidifier temperature ($T_H$) required to maintain the desired relative humidity of the mixed gas stream at the cell inlet ($\phi$) is described by Eq. (1). The humidifier temperature depends on the saturation pressure of water in the cell $P^{Sat}_w(T_C)$ at the cell temperature ($T_C$), the neat ($\dot{n}_{g,M}$) and contaminated ($\dot{n}_{g,I}$) molar gas flow rates and the cell pressure ($P_{Cell}$). Saturation pressures were determined with the Antoine equation and values for $T_H$ were iteratively determined using Eq. (1). When there is no impu-

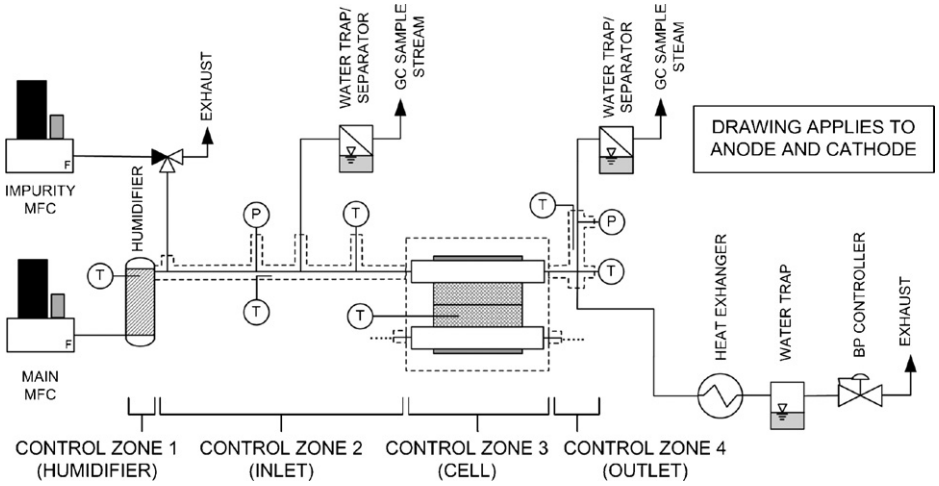


**Fig. 1.** Schematic of gas flow, pressure and temperature control of experimental setup including positioning of sampling lines for gas analysis.

rity, the flow of the impurity containing mixture ($\dot{n}_{g,I}$) becomes zero and Eq. (1) simplifies to Eq. (2).

$$P_w^{Sat}(T_H) = \left[\frac{\phi \cdot P_w^{Sat}(T_C)(\dot{n}_{g,M} + \dot{n}_{g,I})}{\dot{n}_{g,M} \cdot (P_{Cell} - \phi \cdot P_w^{Sat}(T_C)) + (\phi \cdot P_w^{Sat}(T_C)(\dot{n}_{g,M} + \dot{n}_{g,I}))}\right] P_{Cell} \quad (1)$$

$$P_w^{Sat}(T_H) = \phi P_w^{Sat}(T_C) \quad (2)$$

To validate the humidification strategy and control, cell performance and resistance were monitored while non-humidified neat hydrogen was injected into the humidified main $H_2$ gas stream. A typical gas mixing ratio of 1:20 was used to simulate an impurity experiments. Cell performance and cell resistance were found to be unaffected and additional dew point sensor experiments confirmed the humidification of the gas remained constant when injecting gas into the main gas stream.

The gas temperature in control zone 2 near the anode inlet, was maintained at 2 °C above the cell temperature to prevent condensation in the stainless steel tubing, connectors and fittings. The thermocouple for control zone 2 was located in the gas stream within 6 cm of the cell inlet.

Control zone 3 in Fig. 1 represents the temperature control region for the fuel cell. Thermocouples were placed inside the flow-field blocks and the temperature control point for the cell was the cathode flow-field. A PID temperature controller with silicon pad heaters adhered to the endplates of the fuel cell hardware enabled to control the cell temperature to within ±0.2 °C of the selected cell temperature.

The surface temperature of the exhaust tubing downstream from the cell (control zone 4), was maintained approximately 10 °C above the cell temperature, to prevent water condensation at the gas sampling points. Further downstream, past control zone 4, heat exchanger systems and water traps were installed to condense and remove most of the effluent water allowing stable pressure control using Type 2000 Marsh Bellofram pressure controllers and Tescom backpressure regulators.

Fig. 1 also shows the gas sampling lines which were located approximately 11 and 5 cm from the fuel cell inlet and outlet ports, respectively. A small fraction of the total gas flow was diverted to the gas analyzer flowing through teflon membrane water traps (United Filtration Systems, SM105.221.M1) and ca. 10 m long sulfinert coated 1/16 inch o.d. stainless steel lines before entering the gas analysis system. Needle valves located at the exit of the GC were used to control the gas flow to the GC to 50–60 $cm^3$ for the $H_2$ and 20–30 $cm^3$ for the air stream measured with the Varian intelligent digital flowmeter. Analysis of the samples took 9.5 min. Sample gas was flowed for an additional 6 min to purge the GC system between samples, allowing sampling approximately every 15 min.

Careful analysis of the gas sample showed that it was not possible to remove all the water in the gas sampling lines with the teflon membrane water traps. Subsequently, a correction to accurately determine the water remaining in the gas sample was developed. At low (ppm and below) contaminant levels, this correction was essential for accurate measurements. Details of this procedure are described in Section 4.

The gas analyzer consisted of two Varian 3800 gas chromatographs which housed a flame ionization detector (FID), a pulsed flame photometric detector (PFPD), a dual thermal conductivity detector (TCD) and a pulsed discharge ionization detector (PDID). The detection limits of the various detectors for species of interest including several gases commonly used for fuel cell operation are shown in Table 1. During experiments, calibration gases from Matheson TriGas were analyzed every 6 h for calibration. Table 2 lists the calibration gases and their certification accuracy. Analysis of the GC data showed that the instrument operated well within its specifications including peak area reproducibility <2%, calibration reproducibility <±3% and reduction catalyst efficiency >95%.

The analyzer was equipped with a programmable 31 port auto-sampling valve allowing fully automated sampling from 31 locations on the various test stands. The sampling valve assembly was heated to 120 °C. In addition to its use for the contaminant stud-

**Table 1**
Detection limits of gas analysis system.

| Impurity | Detector | Detection limit |
|---|---|---|
| $H_2S$ | PFPD | 50 ppb |
| $SO_2$ | PFPD | 50 ppb |
| COS | PFPD | 50 ppb |
| CO | PDID | 100 ppb |
| CO | FID | 100 ppb |
| $CO_2$ | FID | 100 ppb |
| $C_3H_8$ | FID | 500 ppb |
| $C_6H_6$ | FID | 500 ppb |
| $C_7H_8$ | FID | 500 ppb |
| $O_2$ | PDID | 10 ppm |
| $N_2$ | PDID | 10 ppm |
| $H_2$ | TCD | 100 ppm |

**Table 2**
Calibration gases, impurity concentration and gas certification accuracy.

| Calibration gas in $H_2$ balance | Impurity concentration (ppm) | Certification accuracy (%) |
|---|---|---|
| $CO/CO_2$ | 1 | 5 |
| | 10 | 5 |
| | 50 | 2 |
| Toluene ($C_7H_8$) | 249 | 2 |
| Benzene ($C_6H_6$) | 100 | 2 |
| | 1000 | 2 |
| Propane ($C_3H_8$) | 10 | 5 |

**Table 3**
Cell hardware.

| Hardware | General | |
|---|---|---|
| | Anode | Cathode |
| Hardware | OEM provided [44] | |
| Flow-field | 2 channel serpentine | 3 channel serpentine |
| MEA | Ion Power (CO exps.) | |
| | GORE™ PRIMEA® (Toluene exps.) | |
| Area | 50 $cm^2$ | |
| Catalyst | 50% Pt/C | 50% Pt/C |
| Loading | 0.4 mg Pt $cm^{-2}$ | 0.4 mg Pt $cm^{-2}$ |
| GDL | SGL-BC25 (CO exps.) | |
| | SGL-BC20 (Toluene exps.) | |
| Gaskets | 178 μm, Teflon | 203 μm, Teflon |

ies, facility gases such as air, $N_2$, and $H_2$ were injected 3–4 times per week to verify their quality.

All trace gases detected by the gas analyzer were measured in parts per million (ppm). This is an inconvenient unit for directly quantifying the reaction processes, since the concentration of the contaminant species changes with the concentration of the fuel or oxidant gas. For example, at the chosen fuel stoichiometry of 2, 50% of the $H_2$ reacts in the fuel cell, and the concentration of any constituent that passes through the cell doubles when comparing inlet to outlet concentration. To quantify the reaction of a contaminant and its reaction products, as described in Section 3, the molar flow rates were used. The molar flow rates were determined from the concentrations of the species detected in the gas sample streams, the total gas flow rates into and out of the cell, and the presence of residual water in the gas sample stream. Further details are given in Section 4.1.

Test procedures used in this work complied with the draft procedures presented at the ISO TC197 working group 12 (WG12) meeting on hydrogen quality in Honolulu, Hawaii, November 2006 [39]. All experiments were conducted using 50 $cm^2$ single cell hardware with double and triple serpentine flow-fields on anode and cathode, respectively. Ion Power membrane electrode assemblies (MEAs) were used for the CO studies while GORE™ PRIMEA® MEA Series 5510[2] were used for the toluene studies. Sigracet SGL-BC25 and Sigracet SGL-BC20 gas diffusion layers (GDLs) were employed, respectively. Cell geometry, catalyst type, catalyst loading, and gasket type and thicknesses were not varied between experiments. The hardware and materials, and standard operating conditions used in this work are listed in Tables 3 and 4, respectively.

Original equipment manufacturer (OEM) provided protocols were used for cell build and conditioning. All cells were leak checked to verify cell assembly. Following cell conditioning, cell diagnostics (described below) were performed and required to match the typical MEA results before any experiments were initiated. The effect of contaminants was characterized by comparing

[2] GORE, CARBEL, GORE-SELECT, PRIMEA and designs are trademarks of W.L. Gore & Associates, Inc.

**Table 4**
Standard experimental conditions.

| Operating conditions | General | |
|---|---|---|
| | Anode | Cathode |
| Relative humidity | 100% | 50% |
| Stoichiometry | 2 | 2 |
| Fuel/oxidant | $H_2$ | Air |
| Backpressure | 48.3 $kPa_g$ | |
| Temperature | 60 °C | |
| Current density[a] | 1 A $cm^{-2}$ | |

[a] Standard for constant current hold experiments.

the change in cell voltage under constant current operation in the presence of an impurity to the cell voltage expected from operation using neat $H_2$ [40]. Each experiment consisted of three phases: (i) an initial period operating with neat $H_2$, (ii) operation with a controlled concentration of contaminant in the $H_2$ fuel, and (iii) a recovery phase using neat $H_2$.

The initial experiments were conducted to characterize the effect of trace amounts of CO in the $H_2$ fuel at our standard conditions of 1 A $cm^{-2}$ and 80 °C. However, testing under neat $H_2$ conditions showed unexpected and significant amounts of $CO_2$ on both the anode and cathode side of the fuel cell. $CO_2$ was the only trace species detected in either gas stream during these tests. Fig. 2(a) and (b) show the molar flow rates of $CO_2$ at the inlet and outlet of the cathode and anode, respectively, over a 100 h period during which each port was sampled at 5 h intervals. Fig. 2(a), shows that the molar flow rate of $CO_2$ at the cathode fluctuated from 0 to 0.42 μmol $s^{-1}$. The latter value corresponds to a measured concentration at the cathode inlet of 340 ppm $CO_2$. The time dependence of the $CO_2$ molar flow rates in Fig. 2(a) and (b) show a strong correlation between the anode outlet and the cathode inlet and outlet values but no correlation with the anode inlet values. This was interpreted as diffusion of $CO_2$ across the membrane from the cathode to the anode. The maximum value of the molar flow rate of $CO_2$ at the anode outlet, 0.0016 μmol $s^{-1}$, corresponds to a concentration of 6 ppm $CO_2$, far below the maximum values recorded at the cathode.

Subsequent effort to determine the cause of $CO_2$ at the cathode showed it to be due to incomplete air clean up resulting from intermittent operation of the pressure swing absorption (PSA) system on the air supply at the HFCTF. The control parameters were changed to force continuous cycling of the PSA. With this change, the $CO_2$ concentration in the air inlet was reduced to less than 1 ppm and remained at that value for all studies presented in this work. The trace amounts of $CO_2$ remaining in the cathode feed stream were attributed to $CO_2$ coming out of solution inside the gas humidifier system. These preliminary experiments clearly showed the need to monitor the gas composition of the inlets and exits of both the anode and cathode side of the fuel cell to ensure full understanding of the processes that occur within the cell. They also showed the importance of thoroughly controlling gas clean-up for successful closure of the contaminant molar flow balances.

Contamination experiments were performed by injecting fixed concentrations of CO or toluene into the anode feed stream. Contaminant concentrations were measured in both inlet and outlet streams with a GC. The measured concentrations were converted to molar flow rates which were used to identify the reaction chemistry and quantify the extent of reaction within the cell at steady state conditions. CO was injected at concentrations of 1, 2, and 10 ppm at an operating temperature of 60 °C, while toluene concentrations of 20, and 60 ppm were injected at cell temperatures of 60 and 80 °C, respectively. With exception of the toluene experiment at 80 °C all operating conditions were set to the standard conditions listed in Table 4.

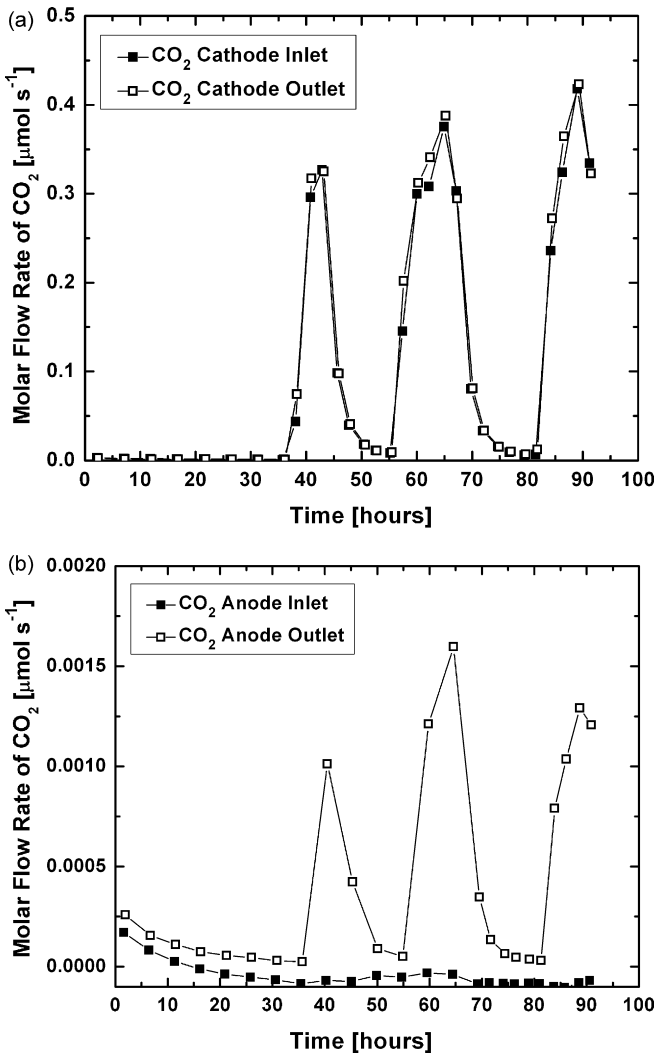


**Fig. 2.** (a) $CO_2$ mole fraction fluctuations at the cathode during experiment at 80 °C, and 1 A cm$^{-2}$. (b) $CO_2$ mole fraction fluctuations at anode due to $CO_2$ crossover.

## 3. Results

In this section, we summarize the results of experiments conducted to characterize the effects of CO and toluene on cell performance while simultaneously identifying the reaction chemistry and quantifying the extent of reaction of the contaminant within the cell. As described in the preceding section, this was accomplished by carefully measuring the composition of the inlet and outlet gases at the anode and cathode. The GC data was corrected for the presence of residual water in the gas sample, a procedure that is discussed in Section 4.

Fig. 3 shows the voltage response of the test cell operated at standard operating conditions when 1 ppm CO is present in the anode feed stream. CO was injected after 45 h of operation on neat hydrogen. Injection was performed continuously for 55 h. During injection, the cell voltage decreased by approximately 175 mV over the first 35 h at which time the cell voltage stabilized. Once the cell voltage had stabilized, CO and $CO_2$ concentrations were measured at approximately 15 min intervals over a time period of about 13 h. Cell recovery was initiated at 100 h by stopping the injection of CO. During recovery, the cell voltage initially increased rapidly and then appeared to asymptotically approach the value prior to poisoning. After 30 h of recovery (i.e. 130 h into the test), the anode had recovered 95% of the change in cell voltage.

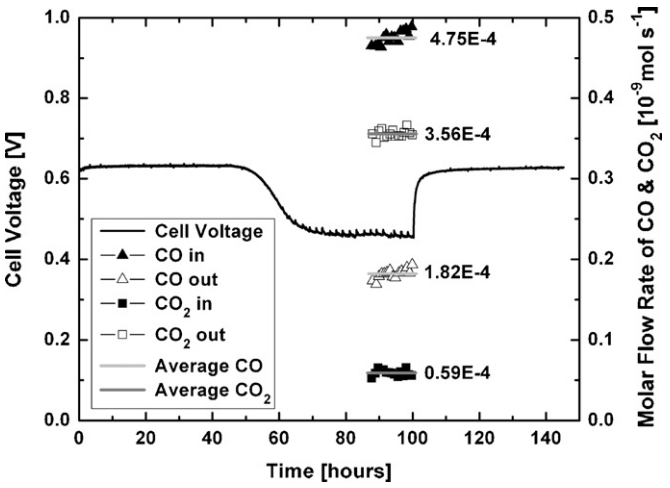


**Fig. 3.** Cell voltage response to exposure of 1 ppm CO at the anode at 60 °C and 1 A cm$^{-2}$ and molar flow rates of CO and $CO_2$ at steady state poisoning conditions.

The molar flow rates of CO and $CO_2$, calculated using the GC data, for the inlet and exhaust streams of the anode during this period are also shown in Fig. 3. It is important to note that $CO_2$ was present in the fuel inlet stream, at a molar flow rate of $0.059 \times 10^{-9}$ mol s$^{-1}$. As described in the previous section, this was attributed to $CO_2$ coming out of solution in the anode humidifier and entering the cell. The molar flow rate of $CO_2$ in the anode exhaust stream was found to be almost one order of magnitude higher ($0.356 \times 10^{-9}$ mol s$^{-1}$) than that at the inlet, while the molar flow rate of CO at the outlet ($0.182 \times 10^{-9}$ mol s$^{-1}$) was significantly lower than at the inlet ($0.475 \times 10^{-9}$ mol s$^{-1}$). This change in the molar flow rates of CO and $CO_2$ from the inlet to the outlet of the anode indicated significant conversion of CO to $CO_2$ within the cell.

However, in order to quantify the extent of reaction accurately, the molar flow balance of the contaminant and its reaction products was required to close at steady state. Closure of the carbon balances at steady state $Q_{CBal}$ was calculated using Eq. (3), where $\bar{n}_{i,out}$ represented the total molar flow rate of impurity species out of the electrode and $\bar{n}_{i,in}$ was the total molar flow rate of species into the respective electrode. A value of one indicates complete closure of the molar flow balance of carbon at the anode. The average molar flow rates following voltage stabilization (i.e. between 87 and 100 h for the experiment shown in Fig. 3) were used to calculate closure.

$$Q_{CBal} = \frac{\sum_i \bar{n}_{i,out}}{\sum_i \bar{n}_{i,in}} \quad (3)$$

For the example experiment shown in Fig. 3, the balance closed to 100.6%. Table 5 lists the results from CO experiments conducted at other inlet concentrations of 2 and 10 ppm. The carbon balances for these experiments closed between 97.7% and 100.6%. The closure of the carbon balance at steady state allowed accurate calculation of the extent of reaction which increased from 61.7% to 91.3% as the CO concentration increased from 1 to 10 ppm.

**Table 5**
Extent of reaction and percentage carbon balance quality for fuel stream impurities.

| Temperature (°C) | Contaminant and concentration | Reaction product | Extent of reaction | $Q_{CBal}$ |
|---|---|---|---|---|
| 60 | 1 ppm CO | $CO_2$ | 61.7% | 100.6% |
| 60 | 2 ppm CO | $CO_2$ | 70.3% | 98.0% |
| 60 | 10 ppm CO | $CO_2$ | 91.3% | 97.7% |
| 60 | 20 ppm $C_7H_8$ | $C_7H_{14}$ | 98% | 100.4% |
| 80 | 60 ppm $C_7H_8$ | $C_7H_{14}$ | 97.0% | 96.9% |

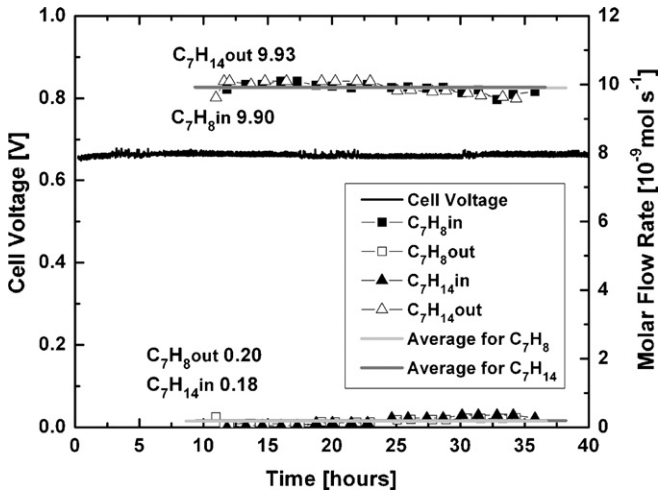


**Fig. 4.** Cell voltage response to exposure of 20 ppm toluene at 60 °C and 1 A cm$^{-2}$ and molar flow rates of toluene ($C_7H_8$) and methylcyclohexane ($C_7H_{14}$).

Table 5 also summarizes the results of two experiments conducted using toluene ($C_7H_8$) as the anode contaminant. Similarly, excellent closure of the mass balance was found (96.9–100.4%) confirming the very high quality of the data. As discussed in more detail below, the extent of reaction of toluene to methylcyclohexane ($C_7H_{14}$) was even higher than that for CO to $CO_2$. Sample results with toluene as the contaminant are shown in Fig. 4 which shows the cell voltage response and toluene and methylcyclohexane molar flow rates at steady state for a fuel cell exposed to 20 ppm toluene. No significant change in cell performance was observed during toluene exposure. The measured cell voltage degradation rate of 47 μV h$^{-1}$ was typical for cells operated in this laboratory with pure hydrogen at identical operating conditions. This suggests that, at the given operating conditions, toluene did not act as a poison to the cell. However, as shown in Fig. 4, the GC analysis of the anode gas stream shows that a hydrogenation of toluene ($C_7H_8$) into methylcyclohexane ($C_7H_{14}$) occurred within the fuel cell. The extent of this reaction (98%) is indicative of almost complete conversion. The reaction of toluene to methylcyclohexane was verified using solid phase microextraction absorption (SPME) techniques coupled with gas chromatograph/mass spectrometry (GC–MS).

For both CO and toluene contamination, the near complete closure of the molar flow balance at steady state implies that the rate of adsorption of the impurity species is equal to the combined desorption and reaction rates (oxidation or hydrogenation, respectively). The significant decrease in cell voltage due to CO exposure implies high surface coverage of CO on the catalyst surface, while the significant extent of reaction of CO to $CO_2$, assuming a negligible amount of oxygen present at the anode, suggests the primary mechanism for CO removal from the catalyst surface being the electro-oxidation of CO to $CO_2$. This reaction requires an oxygen atom which has been assumed to originate from the discharge of a water molecule [22]. The combined desorption/reaction of CO is sufficiently slow to result in significant coverage of the Pt active sites hence a significantly reduced rate of the hydrogen oxidation reaction (HOR) and detrimental impact on fuel cell performance [1].

For the catalytic hydrogenation of toluene to methylcyclohexane various reaction models have been reported in the literature suggesting that the rate limiting step may be the addition of the first hydrogen atom or the first $H_2$ molecule to the aromatic ring [43], while others suggest comparable rates for the individual reaction steps [43]. While the work here does not provide insights into the rate limiting step, the nearly complete conversion of toluene to methylcyclohexane combined with the negligible impact on the HOR of the fuel cell, even at an elevated concentration of 60 ppm toluene, indicates a rapid hydrogenation–desorption sequence. Therefore, we assumed that the reaction rate for the hydrogenation of toluene was consequently much faster than that of the CO electro-oxidation and it can be expected that the residence time of toluene on Pt was much lower than that of CO. Additional work is underway to characterize the extent of reaction under a wider range of operating conditions. These data will be used to develop models to determine rate constants for the various reactions involved.

## 4. Discussion

In order to accurately quantify conversion and reaction processes within the fuel cell, the molar flow balance of the contaminant species and its reaction products must close at steady state conditions. As shown in this section, the molar flow rate of each contaminant species entering and exiting the cell in the anode and cathode streams was calculated from the gas flow rates, the fuel or oxidant stoichiometry, and the concentration of each of the trace species at the four sample ports which was measured by the GC. However, the accuracy of the GC measurement may be affected by two possible sources of systematic errors: (i) the dissolution of impurity species into liquid water and (ii) the incomplete removal of water from the sample stream entering the GC. Both possible errors were studied and are discussed in this section.

### 4.1. Species solubility in water

The amount of contaminant capable of dissolving into liquid water was estimated using Henry's Law given in Eq. (4), which was valid since the system was held at constant temperature and pressure and the impurity species were present in small amounts [41,42]. Expressed in the form of Eq. (4), Henry's law defined the ratio of the concentration of a species $c_i$ dissolved in a liquid to the partial pressure over the liquid of the same species $p_i$ to be related by Henry's constant $k_{H,i}$. This constant was dependent on the system temperature as given in Eq. (5) where $\Delta H$ represented the change in enthalpy of solution, $R$ the ideal gas constant, $T$ the system temperature, $T^{\circ}$ the reference temperature (25 °C for this case), and $k^0_{H,i}$ the value for Henry's constant at reference conditions.

$$k_{H,i} = \frac{c_i}{p_i} \tag{4}$$

$$k_{H,i} = k^0_{H,i} \exp\left(\frac{-\Delta H}{R}\left(\frac{1}{T} - \frac{1}{T^0}\right)\right) \tag{5}$$

The Henry's constants for various fuel cell contaminants at practical operating temperatures were calculated and listed in Table 6. Constants were typically determined at a particular temperature by averaging two literature values for $k^0_{H,i}$ and $(-\Delta H/R)$ from Sander [42]. With this data, the concentration of the impurities that could dissolve in the product water was estimated with Eq. (4), assuming liquid water production at the cathode as the only source of liquid water, and assuming full access to this water for dissolution of anode and cathode impurities. At cell operating temperatures of 60 °C, a cell current density of 1 A cm$^{-2}$, and impurity concentrations of 10 ppm, the highest reduction in CO and $CO_2$ concentration that could occur were 0.17 and 4.01 ppb, respectively. For 60 ppm toluene and methylcyclohexane, the respective values were and 59.46 and 0.60 ppb, respectively. All these values were significantly below the detection limits of the GC shown in Table 1.

Impurity species dissolution into liquid product water therefore did not have any measurable effects on the results presented in this work. However, since Henry's constant is temperature dependent and for CO and $SO_2$ varies at the same temperatures by approxi-

**Table 6**
Henry's law constants for solute species in liquid water as a function of temperature (units: mol dm$^{-3}$ atm$^{-1}$) [42].

| $T$ (°C) | $O_2$ | $H_2$ | $SO_2$ | Benzene | Toluene | MCH[a] | CO | $CO_2$ |
|---|---|---|---|---|---|---|---|---|
| 25 | 1.3E−03 | 7.8E−04 | 1.4E+00 | 1.6E−01 | 1.5E−01 | 9.6E−03 | 9.7E−04 | 3.5E−02 |
| 60 | 7.7E−04 | 6.6E−04 | 5.1E−01 | 3.8E−02 | 3.7E−02 | 3.7E−04 | 6.1E−04 | 1.5E−02 |
| 70 | 6.7E−04 | 6.3E−04 | 4.0E−01 | 2.6E−02 | 2.6E−02 | 1.6E−04 | 5.5E−04 | 1.2E−02 |
| 80 | 5.9E−04 | 6.0E−04 | 3.2E−01 | 1.9E−02 | 1.9E−02 | 7.6E−05 | 4.9E−04 | 9.8E−03 |

[a] MCH = methylcyclohexane.

mately three orders of magnitude (Table 6), dissolution of impurity species should be considered on a case by case basis.

### 4.2. Impact of water in the GC sample stream

In addition to dissolution of contaminants into liquid product water inside the cell, incomplete water removal from the gas sample stream was investigated as another source of systematic error. Any gas sample analyzed by the GC in this work consisted of a mixture of the reactant gas, $CO_2$, water vapor, and the injected impurity (i.e. toluene or CO). Accurate quantification of the impurity species in the gas streams required quantification of all the species in the gas stream. This presented a challenge because although the GC had detection limits for $CO_2$, CO, and hydrocarbons in the ppb range (Table 1), calibration curves were based on dry gas standards and the ability of the GC to quantify the concentration of water was limited to a percentage resolution. Since more accurate quantification of water was required for this work, water traps were introduced into the GC sample stream, as shown in Fig. 1, to reduce the amount of water entering the GC to negligible amounts and measure the concentrations of impurities in the dry gas. As shown in Fig. 5(a), however, due to these water traps, the mole fraction of water entering the GC ($y_{w_2}$) was not equivalent to the mole fraction of water entering the cell ($y_{w_1}$). Instead, the GC data represented mole fractions that would exist if an identical water trap was placed upstream of the cell, as shown in Fig. 5(b). To determine the exact impurity molar flow rates from the concentrations measured by the GC, the impact of the water trap on the GC measurement was determined. In the following Section 4.2.1, the strategy to identify the effectiveness of the water traps at different operating conditions and to correct the measured concentrations of $CO_2$, CO, toluene, and methylcyclohexane for the presence of water in the sample stream is described. Subsequently in Section 4.2.2, the essential calculations are discussed in more detail.

#### 4.2.1. Correction method

Fig. 6 shows the concentrations of CO measured with the GC during constant injection of 1 and 2 ppm CO while increasing the amount of water in the sample stream by increasing the humidifier temperature. When humidifier temperatures exceeded approximately 65 °C, the mole fractions of CO were observed to decrease significantly and non-linearly. The data indicates that the amount of water entering the GC via the sample stream was not constant and not negligible, but increased with the amount of water in the main gas stream. With increasing amounts of water in the GC sample stream the measured concentration of CO and $CO_2$ decreased from their respective concentrations entering the cell. Since the effectiveness of the water trap used in this work was not improved by submerging it in an ice bath, the presence of water entering the GC needed to be accounted for. This was accomplished in three steps:

1. Fitting the data in Fig. 6 and assuming that the change in CO concentration was only caused from additional water passing the water trap and entering the GC.
2. Obtaining an empirical relationship between the amount of water entering the cell if an identically effective water trap was placed in the feed stream (known from GC data and fit) and the actual amount of water entering the fuel cell (known from humidifier temperature and gas flow rates).
3. Determining the actual amount of water entering the GC, correcting the concentrations measured by the GC to dry gas values, and calculating the actual molar flow rates of the impurity and $CO_2$ in the gas streams.

Fig. 7 shows the relationship between the molar flow rate of water entering the cell assuming a water trap was placed upstream of the cell and the actual molar flow rate of water entering the cell. Both data sets were fitted to a single empirical equation, which was applied for data correction and accounted for the presence of water in the gas sample stream. This enabled an accurate determination of the molar flow rates of the impurities and $CO_2$.

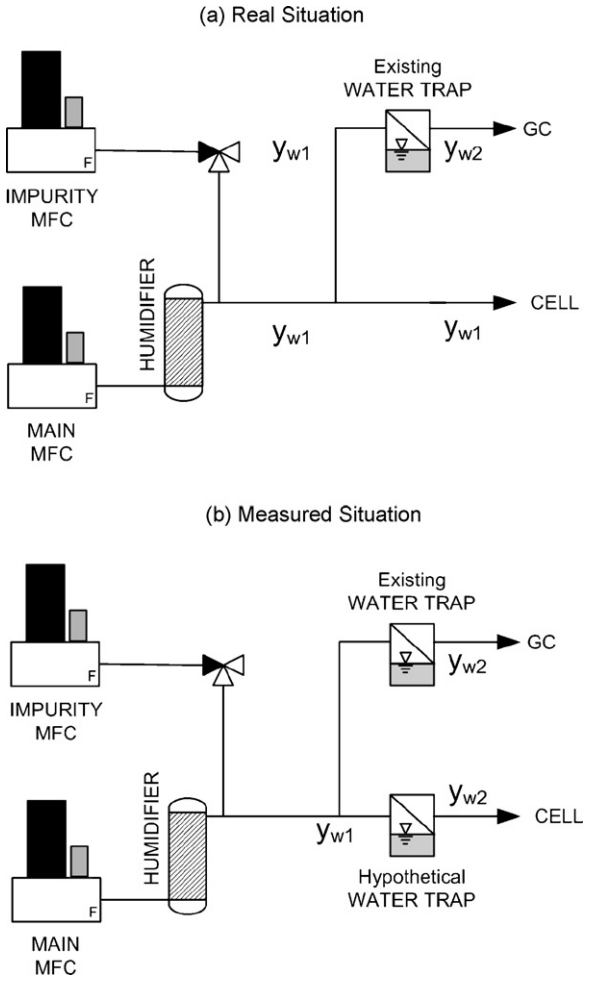


**Fig. 5.** Schematic of the impact of the water traps in the gas sample streams on the experiment: (a) experimental (real) situation and (b) measured situation. The mole fraction of water entering the GC $y_{w_2}$ differs from the actual mole fraction of water entering the cell $y_{w_1}$. A hypothetical water trap in the inlet stream is used to calculate the molar flow rates of the impurity species entering the fuel cell from the GC data.

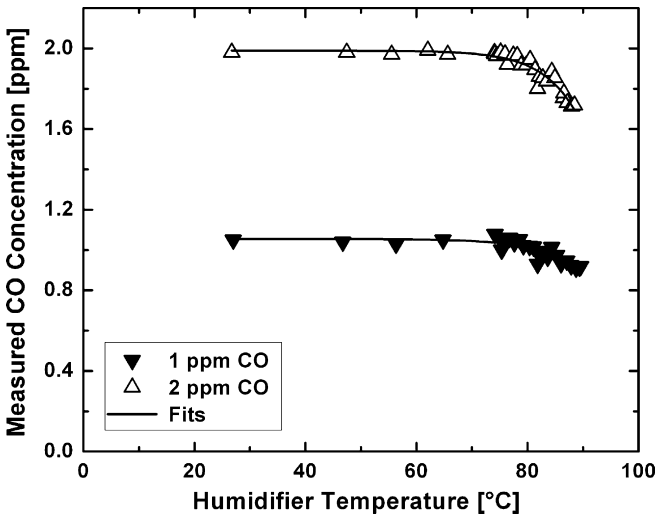


**Fig. 6.** Measured CO concentration vs. humidifier temperatures for 1 and 2 ppm CO using constant flow rates for CO injection and main gas stream.

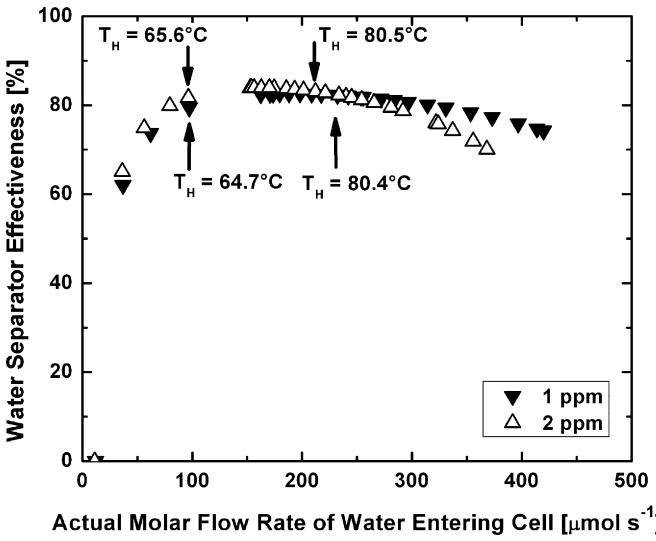


**Fig. 8.** Water separator effectiveness vs. molar flow rate of water entering the fuel cell for 1 and 2 ppm CO injection.

Fig. 8 shows the effectiveness of the water trap vs. molar flow rate of water present in the mixed gas stream. The water separator was least effective when molar flow rates of water corresponded to conditions near saturation at ambient temperatures. This was expected, since the temperature differential between the gas sample stream and the water separator were small. The data in Fig. 8 indicated that for molar flow rates of water ranging from 100 to 300 μmol $s^{-1}$ above 80% of the water was removed from the gas sample stream. However, since more water entered the water trap, more water also passed through the water trap and entered the GC. At even higher molar flow rates the relative amount of water removed by the water trap declined for both experiments at different rates. The slight deviation of the data sets was attributed to data collection during ramping of the humidifier temperature.

The impact of implementing the corrective equation is shown in Fig. 9, which compares the corrected data previously shown in Fig. 2(a) with the uncorrected data for the cathode outlet. The uncorrected data indicated a loss of $CO_2$ at the cathode. However, the majority of the apparent loss shown in Fig. 9 was artificial and was in fact due to water entering the GC. Only a small portion of $CO_2$ (0.0016 μmol $s^{-1}$) was exiting the cathode flow stream by diffusing to the anode as shown by Fig. 2(a) and (b). This emphasizes the importance of implementing the corrective equation for the presence of water entering the GC so that accurate results can be obtained.

*4.2.2. Corrective equation*

In this subsection, the equations that were applied to correct the GC data and calculate the actual molar flow rates entering or exiting the cell are derived and discussed. Eq. (6) shows that the concentration of a species in a gas stream in units of ppm, $y_{s,ppm}$ can be expressed by the molar flow rate of this species $\dot{n}_s$ multiplied by $1 \times 10^6$ and divided by the sum of all the molar flow rates $\dot{n}_j$ in the gas stream. Solving this equation for the molar flow rates in units of mol $s^{-1}$ of either an impurity or $CO_2$ yields Eq. (7) or Eq. (8), respectively, where $\dot{n}_i$ and $\dot{n}_{CO_2}$ were the molar flow rates of the impurity and $CO_2$, respectively, and $a_i$ and $a_{CO_2}$ were conversion factors used to convert the concentrations measured by the GC for the impurity $y_{i,ppm}$ and for $CO_2$ $y_{CO_2,ppm}$ from ppm to full scale. $\dot{n}_{w,Hyp}$ was the flow rate of water into the fuel cell with a hypothetical water trap identical to the water trap in the GC sample stream had been placed

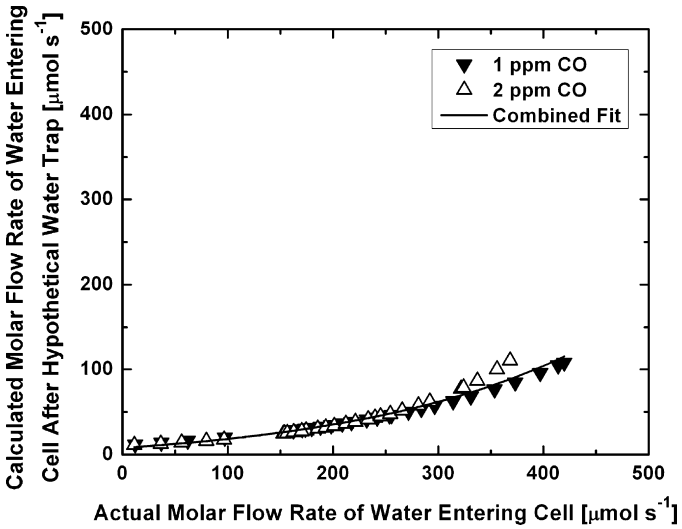


**Fig. 7.** Molar flow rate of water calculated from GC data plotted vs. the actual molar flow rate of water entering the fuel cell for 1 and 2 ppm CO injection.

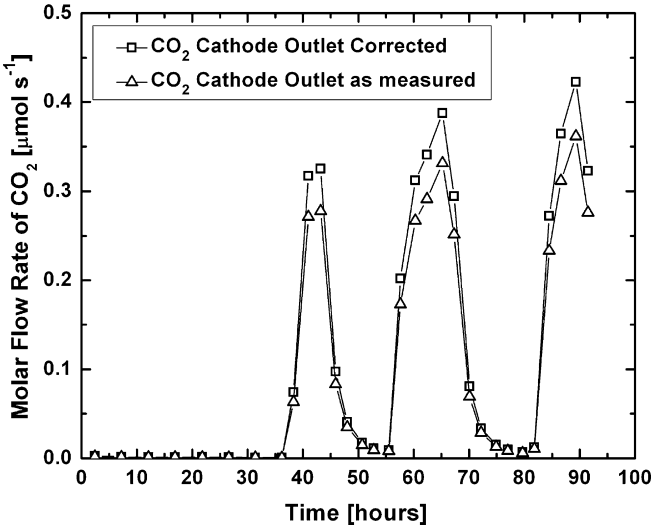


**Fig. 9.** Fluctuations of $CO_2$ molar flow rate at the cathode prior to (-□-) and after (-△-) correction for the presence of water in the GC sample stream.

**Table 7**
Humidifier temperatures and outlet saturation temperatures at standard operating conditions and cell temperatures of 60 and 80 °C.

| Cell temperature (°C) | Electrode | Inlet relative humidity (%) | Humidifier temperature $T_H$ (°C) | Outlet saturation temperature $T_{Sat}$ (°C) |
|---|---|---|---|---|
| 60 | Anode | 100 | 60.0 | 63.2 |
| 60 | Cathode | 50 | 45.8 | 66.6 |
| 80 | Anode | 100 | 80.0 | 81.5 |
| 80 | Cathode | 50 | 64.0 | 80.2 |

in the feed stream of the cell. $\dot{n}_{w,Hyp}$ was the only unknown in Eqs. (7) and (8), and needed to be determined to correct the GC data for the water in the gas sample stream. The molar flow rates for the reactant gas streams at the cell inlet $\dot{n}_{r,In}$ and outlet $\dot{n}_{r,Out}$ in units of mol s$^{-1}$ were calculated from the selected reaction stoichiometry λ using Eqs. (9) and (10), respectively, where $\alpha$ was the known fraction of the fuel or oxidant in the gas stream (e.g. in normal air $\alpha$ is equal to 0.21), $I$ the cell current in the experiment, $n$ the number of electrons transferred during the electrochemical reaction at either the anode or cathode (i.e. two for the HOR and four for the oxygen reduction reaction (ORR)), and $F$ Faraday's constant.

$$y_{s,ppm} = \frac{1 \times 10^6 \cdot \dot{n}_s}{\sum_j \dot{n}_j} \tag{6}$$

$$\dot{n}_i = \frac{a_i}{1 - a_i \cdot a_{CO_2}} \cdot [\dot{n}_{r,In/Out} + \dot{n}_{w,Hyp} + (\dot{n}_{r,In/Out} + \dot{n}_{w,Hyp}) \cdot a_{CO_2}] \tag{7}$$

Eq. in units of mol s$^{-1}$.

$$\dot{n}_{CO_2} = \frac{a_{CO_2}}{1 - a_{CO_2} a_i} [\dot{n}_{r,In/Out} + \dot{n}_{w,Hyp} + (\dot{n}_{r,In/Out} + \dot{n}_{w,Hyp}) \cdot a_i] \tag{8}$$

where $a_i = y_{i,\mathrm{ppm}}/(1 \times 10^{-6} - y_{i,\mathrm{ppm}})$; $a_{CO_2} = y_{CO_2,\mathrm{ppm}}/(1 \times 10^6 - y_{CO_2,\mathrm{ppm}})$.
Eq. in units of mol s$^{-1}$.

$$\dot{n}_{r,In} = \frac{\lambda I}{nF\alpha} \tag{9}$$

$$\dot{n}_{r,Out} = \frac{(\lambda - \alpha) I}{nF\alpha} \tag{10}$$

The unknown $\dot{n}_{w,Hyp}$ was determined by solving Eq. (7) to obtain Eq. (11) and using the data of the measurements shown in Fig. 6, which quantified the impact of water on the experimental results. The molar flow rate of CO into the cell $\dot{n}_{CO}$ was known from the selected flow rates of the injected gas stream and the main gas stream. The values for $a_{CO}$ in Eq. (11) were determined by fitting the GC data when plotted vs. the calculated actual amount of water $\dot{n}_{w,act,In}$ entering the cell, while values for $a_{CO_2}$ were taken directly from the experimental results.

$$\dot{n}_{w,Hyp} = \left( (1 + a_{CO_2})^{-1} \left[ \left( \frac{\dot{n}_{CO}}{a_{CO}} \right) - (1 + a_{CO_2}) \dot{n}_{r,In/Out} \right] \right) \tag{11}$$

In Fig. 7 $\dot{n}_{w,Hyp}$ is plotted vs. $\dot{n}_{w,act,In}$, the actual molar flow rate of water into the cell. Both data sets were fitted to a single empirical equation given by Eq. (12), which related $\dot{n}_{w,Hyp}$ to the actual amount of water $\dot{n}_{w,act,In}$ entering the cell. $\dot{n}_{w,Hyp}$ could then be determined from system operating parameters. $\dot{n}_{w,act,In}$ was given by Eqs. (13) and (14) where $y_{w,In}$ represented the mole fraction of water in the fuel cell inlet stream, $P_w^{Sat}(T_H)$ the saturation pressure of water at the humidifier temperature and $P_{Cell,In}$ the pressure of the cell at the inlet. In the inlet case, the molar flow rate $\dot{n}_{In}$ equals the flow rate of clean gas in the main gas stream that passes through the humidifier.

Eqs. (12)–(14) are also valid for the outlet case, where $\dot{n}_{Out}$ equals $\dot{n}_{r,Out}$ which considered the stoichiometry of the reaction and was described by Eq. (10), and $P_{Cell,Out}$ was the outlet pressure. The hardware used in this work had a negligible pressure drop of approximately 3 kPa across the anode at the employed operating conditions, and the value of $P_{Cell,Out}$ was therefore used for all calculation in this work. However, the pressure drop across a fuel cell hardware depends on channel length and cross-section, flow rate, humidification, and other operating conditions. For a significant pressure drop the pressure driven flow rate of the gas sample streams at the inlet and the outlet will differ. This results in different molar flow rates of water into the water traps that can be accounted for by using appropriate values and the same method shown in this work.

Also, in the outlet case of Eqs. (12)–(14), the saturation temperatures of the exit gases $T_{Sat}$ were found to differ from the temperature of the humidifier $T_H$ over a range of operating conditions such as humidifier temperature, flow rates, and inlet relative humidification. Table 7 lists the inlet relative humidity, the humidifier temperature and the resulting saturation temperature at the cell exit for cell temperatures of 60 and 80 °C and otherwise standard operating conditions. At the cathode exit the saturation temperatures increased significantly indicating an increased presence of water in the cathode exhaust stream. For the purpose of gas stream analysis, the fuel cell hardware had to be considered as a second humidifier system running at the saturation temperature of the anode or cathode exit gas. The mole fraction of water in the fuel cell outlet was thus calculated with Eq. (14) and $T_{Sat}$. Consequently, for accurate gas analysis the saturation temperatures at the GC sample ports were determined for several operating conditions before individual correction of anode and cathode outlet data when saturation temperatures exceeded 65 °C.

$$\dot{n}_{w,Hyp} = -10.22894 + 18.13477 \exp \left[ \frac{\dot{n}_{w,act,In/Out}}{217.13476} \right] \tag{12}$$

Eq. in units of μmol s$^{-1}$.

$$\dot{n}_{w,act,In/Out} = \left[ \frac{y_{w,In/Out}}{1 - y_{w,In/Out}} \right] \cdot \dot{n}_{In/Out} \tag{13}$$

$$y_{w,In/Out} = \frac{P_w^{Sat}(T_{H/Sat})}{P_{Cell,In/Out}} \tag{14}$$

Substituting Eq. (12) into Eq. (7) or Eq. (8) yielded the desired corrective equation. This equation converts the concentration measured by the GC into a molar flow rate while correcting the measured GC data for the amount of water in the gas sample stream. The correction was employed for species quantification at the anode and cathode inlet and outlet. This was done for this work whenever humidifier temperatures exceeded 65 °C. As shown in Fig. 6, at lower temperatures $\dot{n}_{w,Hyp}$ did not affect GC values and was therefore neglected when converting the mole fractions measured by the GC into molar flow rates.

## 5. Conclusions

An experimental and analytical methodology has been developed that employs on-line gas chromatography (GC) to identify and quantify the reactions of trace contaminants in PEMFCs. Careful design of the experimental setup and evaluation of the measured data for systematic errors allowed the quantification of impurity gas

species to sub-ppm levels. This enabled (i) the quantification of conversion processes inside the fuel cell during exposure to ppm-level contaminant concentrations at steady state poisoning conditions, and (ii) the detection of species permeating through the membrane electrode assembly (MEA). The method was employed for studying the effects of 1, 2, and 10 ppm CO, and 20 and 60 ppm toluene in the anode feed stream at 60 and 80 °C operating temperatures.

Accurate closure of the molar flow balance of the contaminants and their reaction products at steady state was achieved within ±3% of complete closure. This proved the validity of the methodology and required consideration of two possible sources of errors: (i) The solubility of the impurities in water was considered for this work and determined to be negligible. For future work, impurity dissolution has to be considered on a case by case basis. (ii) The successful closure of the molar flow balance at temperatures above 65 °C required the correction of the measured GC data. At these operating temperatures increased amounts of water passed through the water traps that were placed in the gas sample stream and decreased the concentration measured by the GC. An equation was derived that corrects for residual water in the GC sample streams above 65 °C and converts the concentrations measured by the GC into molar flow rates. This enabled accurate quantification of impurity gas species to sub-ppm levels at all typical operating conditions.

Application of the measurement methodology to the inlets and outlets of the anode and cathode electrodes, allowed low level fuel contaminants to be tracked and quantified within the fuel cell system. This was demonstrated by identifying the reaction and quantifying the extent of reaction of CO to $CO_2$ and toluene to methylcyclohexane in the anode feed stream. The faster hydrogenation of toluene resulted in complete conversion to methylcyclohexane at the catalyst surface with negligible interference on fuel cell performance, while the slower CO conversion to $CO_2$ resulted in poisoning of the anode and significant degradation of cell performance.

Additional work is underway to use the developed methodology to characterize the extent of reaction under a wider range of operating conditions and contaminants. The method is expected to be applicable to studying the reactions of other gaseous fuel and air contaminants, such as other hydrocarbon species, $H_2S$, COS, $SO_2$, and mixtures of selected or all detectable species. To close the molar flow balance for species that are highly soluble in liquid water, such as $SO_2$, the method may require additional effluent water collection and analysis. Closure of the molar flow balance at steady state as shown in this work also enables the study of non-steady state poisoning and recovery processes. This work is in progress and will be presented in future publications.

## Acknowledgements

This work was conducted at the Hawai'i Natural Energy Institute of the University of Hawai'i under Office of Naval Research Grant #N00014-06-1-0086. The authors would like to thank Chuck Fraley for performing the GC data analysis. We gratefully acknowledge Doug Wheeler for fruitful discussions regarding setup and impurity issues.

## References

[1] X. Cheng, Z. Shi, N. Glass, L. Zhang, J. Zhang, D. Song, Z. Liu, H. Wang, J. Shen, J. Power Sources 165 (2007) 739–756.
[2] N.M. Marković, C.A. Lucas, B.N. Grgur, P.N. Ross, J. Phys. Chem. B 103 (1999) 9616.
[3] N.M. Marković, C.A. Lucas, A. Rodes, V. Stamenković, P.N. Ross, Surf. Sci. 499 (2002) L149.
[4] I. Villegas, M.J. Weaver, J. Chem. Phys. 101 (2) (1994) 1648.
[5] K.A. Friedrich, K.-P. Geyzers, U. Linke, U. Stimming, J. Stumper, J. Electroanal. Chem. 402 (1996) 123.
[6] J.M. Feliu, J.M. Orts, A. Fernandez-Vega, A. Aldaz, J. Clavilier, J. Electroanal. Chem. 296 (1990) 191.
[7] H.A. Gasteiger, N.M. Marković, P.N. Ross, E.J. Cairns, J. Phys. Chem. 98 (2) (1994) 617.
[8] H.A. Gasteiger, N.M. Marković, P.N. Ross, J. Phys. Chem. 99 (1995) 8290.
[9] H.A. Gasteiger, N.M. Marković, P.N. Ross, J. Phys. Chem. 99 (1995) 16757.
[10] Z. Jusys, H. Massong, H. Baltruschat, J. Electrochem. Soc. 146 (3) (1999) 1093.
[11] B. Hammer, O.H. Nielsen, J.K. Nørskov, Catal. Lett. 46 (1997) 31.
[12] G.A. Camara, E.A. Ticianelli, S. Mukerjee, S.J. Lee, J. McBreen, J. Electrochem. Soc. 149 (6) (2002) A748.
[13] L. Gubler, G.G. Scherer, A. Wokaun, Phys. Chem. Chem. Phys. 3 (2001) 325.
[14] S. Jiménez, J. Soler, R. Valenzuela, L. Daza, J. Power Sources 151 (2005) 69–73.
[15] J.-D. Kim, Y.-I. Park, K. Kobayashi, M. Nagai, J. Power Sources 103 (2001) 127–133.
[16] T. Ioroi, K. Yasuda, Y. Miyazaki, Phys. Chem. Chem. Phys. 4 (2002) 2337–2340.
[17] M.-C. Yang, C.-H. Hsueh, J. Electrochem. Soc. 153 (6) (2006) A1043–A1048.
[18] F.A. de Bruijn, D.C. Papageorgopoulos, E.F. Sitters, G.J.M. Janssen, J. Power Sources 110 (2002) 117–124.
[19] C.G. Farrell, C.L. Gardner, M. Ternan, J. Power Sources 171 (2007) 282–293.
[20] A.A. Shah, P.C. Sui, G.-S. Kim, S. Ye, J. Power Sources 166 (2007) 1–21.
[21] J. Zhang, H. Wang, D.P. Wilkinson, D. Song, J. Shen, Z.-S. Liu, J. Power Sources 147 (2005) 58–71.
[22] T.E. Springer, T. Rockward, T.A. Zawodzinski, S. Gottesfeld, J. Electrochem. Soc. 148 (1) (2001) A11–A23.
[23] SAE report 2719.
[24] R. Mohtadi, W.-K. Lee, J.W. VanZee, Appl. Catal. B: Environ. 56 (2005) 37–42.
[25] Z. Shi, D. Song, J. Zhang, Z.-S. Liu, S. Knights, R. Vohra, N.Y. Jia, D. Harvey, J. Electrochem. Soc. 154 (7) (2007) B609–B615.
[26] R. Mohtadi, W.K. Lee, S. Cowan, J.W. VanZee, M. Murthy, Electochem. Solid-State Lett. 6 (2003) A272–A274.
[27] F.A. Uribe, S. Gottesfeld, T.A. Zawodzinski, J. Electrochem. Soc. 149 (3) (2002) A293–A296.
[28] R. Halseid, P.J.S. Vie, R. Tunold, J. Power Sources 154 (2006) 343–350.
[29] R. Halseid, P.J.S. Vie, R. Tunold, J. Electrochem. Soc. 151 (3) (2004) A381–A388.
[30] H.J. Soto, W. Lee, J.W. VanZee, M. Murthy, Electrochem. Solid-State Lett. 6 (7) (2003) A133–A135.
[31] K. Punyawudho, S. Shimpalee, W. John, Van Zee, Abs. 0445 212th Meeting of the Electrochemical Society, October 7–12, Washington, DC, USA, 2007.
[32] Y. Garsany, O.A. Baturina, K.E. Swider-Lyons, J. Electrochem. Soc. 154 (7) (2007) B670–B675.
[33] F. Jing, M. Hou, W. Shi, J. Fu, H. Yu, P. Ming, B. Yi, J. Power Sources 166 (2007) 172–176.
[34] J.M. Moore, P.L. Adcock, J.B. Lakeman, G.O. Mepsted, J. Power Sources 85 (2000) 254–260.
[35] M.-C. Yang, C.-H. Hung, J. Electrochem. Soc. 153 (6) (2006) A1043–A1048.
[36] J. Zhang, R. Datta, Electrochem. Solid-State Lett. 6 (1) (2003) A5–A8.
[37] J. Zhang, R. Thampan, R. Datta, J. Electrochem. Soc. 149 (6) (2002) A765.
[38] Z. Qi, C. He, A. Kaufman, J. Power Sources 111 (2002) 239–247.
[39] G. Bender, K. Bethune, D. Wheeler, R. Rocheleau, "Impurity Test Protocol", ISO TC197 Working Group Meeting on Hydrogen Quality, Honolulu, Hawaii, November 09, 2006.
[40] G. Bender, M. Angelo, K. Bethune, S. Dorn, R. Rocheleau, J. Power Sources, in preparation.
[41] S.I. Sandler, Chemical and Engineering Thermodynamics, 2nd ed., Wiley, New York, 1989, pp. 356–359, 433–441.
[42] R. Sander, Compilation of Henry's Law Constants for Inorganic and Organic Species of Potential Importance in Environmental Chemistry (Version 3), 1999, http://www.henrys-law.org.
[43] M. Saeys, M.-F. Reyniers, J.W. Thybaut, M. Neurock, G.B. Marin, J. Catal. 236 (2005) 129–138.
[44] H.A. Gasteiger, S.S. Kocha, B. Sompalli, F.T. Wagner, J. Appl. Catal. B: Environ. 56 (2005) 9–35.